

1 **MutationalPatterns: The one stop shop for the analysis of mutational processes**

2 Freek Manders^{1,2}, Arianne M. Brandsma^{1,2}, Jurrian de Kanter^{1,2}, Mark Verheul^{1,2}, Rurika

3 Oka^{1,2}, Markus J. van Roosmalen^{1,2}, Bastiaan van der Roest^{2,3,4}, Arne van Hoeck^{2,3}, Edwin

4 Cuppen^{2,3} and Ruben van Boxtel^{1,2,*}

5 ¹Princess Máxima Center for Pediatric Oncology, Heidelberglaan 25, 3584CS Utrecht, The

6 Netherlands

7 ²Oncode Institute, Jaarbeursplein 6, 3521 AL Utrecht, The Netherlands

8 ³Center for Molecular Medicine, University Medical Center Utrecht, Utrecht University,

9 Universiteitsweg 100, 3584, CG, Utrecht, The Netherlands

10 ⁴Julius Center for Health Sciences and Primary Care, University Medical Center Utrecht,

11 Utrecht University, Universiteitsweg 100, 3584, CG, Utrecht, The Netherlands

12 *Corresponding author: R.vanBoxtel@prinsesmaximacentrum.nl

13

14

15 **Abstract**

16 **Background**

17 The collective of somatic mutations in a genome represents a record of mutational
18 processes that have been operative in a cell. These processes can be investigated by
19 extracting relevant mutational patterns from sequencing data.

20

21 **Results**

22 Here, we present the next version of MutationalPatterns, an R/Bioconductor package, which
23 allows in-depth mutational analysis of catalogues of single and double base substitutions as
24 well as small insertions and deletions. Major features of the package include the possibility
25 to perform regional mutation spectra analyses and the possibility to detect strand
26 asymmetry phenomena, such as lesion segregation. On top of this, the package also
27 contains functions to determine how likely it is that a signature can cause damaging
28 mutations (i.e., mutations that affect protein function). This updated package supports
29 stricter signature refitting on known signatures in order to prevent overfitting. Using
30 simulated mutation matrices containing varied signature contributions, we showed that
31 reliable refitting can be achieved even when only 50 mutations are present per signature.
32 Additionally, we incorporated bootstrapped signature refitting to assess the robustness of
33 the signature analyses. Finally, we applied the package on genome mutation data of cell
34 lines in which we deleted specific DNA repair processes and on large cancer datasets, to
35 show how the package can be used to generate novel biological insights.

36

37 **Conclusions**

38 This novel version of MutationalPatterns allows for more comprehensive analyses and
39 visualization of mutational patterns in order to study the underlying processes. Ultimately,
40 in-depth mutational analyses may contribute to improved biological insights in mechanisms
41 of mutation accumulation as well as aid cancer diagnostics. MutationalPatterns is freely
42 available at <http://bioconductor.org/packages/MutationalPatterns>.

43

44 **Keywords**

45 R, regional mutation patterns, mutagenic processes, mutational signatures, indels, base
46 substitutions, somatic mutations

47

48 **Background**

49 Mutational landscapes in the genomes of cells are the result of a balance between
50 mutagenic and DNA-repair processes (1). The somatic mutations that shape these
51 landscapes gradually accumulate throughout life in both healthy and malignant cells (2,3).
52 As a result, the complete collection of somatic mutations in the genome of a cell forms a
53 record of the mutational processes that have been active throughout the life of that cell. In-
54 depth analyses of somatic mutations can allow us to better understand the mutational
55 processes that caused them (4).

56

57 First, such analyses can provide insight into the etiology of cancer by identifying mutagenic
58 exposures, which ultimately contribute to the accumulation of cancer driving mutations. For
59 example, we recently identified a mutational pattern caused by a carcinogenic strain
60 of *Escherichia coli* found in the gut of ~20% of healthy individuals (5). This pattern matched
61 mutations found in colorectal cancer driver genes, indicating a direct role in tumorigenesis.
62 Mutational patterns have been systematically determined *in vitro* for many environmental
63 mutagenic agents, which can be used to deduce cancer causes (6). The effects of such
64 agents can also be found *in vivo*. For example, we recently found mutations caused by
65 exposure to the antiviral drug ganciclovir, which patients received to treat a viral infection
66 after a hematopoietic stem cell transplant (7). Second, studying mutational processes can
67 be useful for improved cancer diagnostics. For example, the presence of certain mutational
68 signatures can be used as a functional readout for deficiency of homologous recombination
69 (HR)-mediated double strand break repair (8,9). Cancers with a defect in this repair pathway
70 are selectively sensitive to poly(ADP-ribose) polymerase (PARP) inhibitors, providing a
71 targeted therapy for the patients (10,11).

72 One of the most popular tools to analyze somatic mutation profiles is the
73 R/Bioconductor package MutationalPatterns, which can be used to easily investigate
74 mutation spectra (12–19). It can also be used to identify new signatures in mutation data
75 using Nonnegative Matrix Factorization (NMF) and to determine the contribution of
76 previously defined signatures to a sample using a method known as “signature refitting” (4).
77 However, the original version of this package has several limitations. First, the package is
78 limited to single base substitutions (SBSs) and cannot be used for small insertions and
79 deletions (indels) or double base substitutions (DBSs) even though signatures for these
80 mutation types have recently been identified in large pan-cancer sequencing efforts (13).

81 The package also suffers from signature overfitting when determining the contribution of
82 known patterns to a sample, which can result in too many signatures being attributed (20).
83 Additionally, the package only allows for analyzing spectra for mutations in the entire
84 genome, making it difficult to study the involvement of specific genomic elements, such as
85 enhancers or secondary hairpin structures. The ability to investigate the role of such
86 elements in mutation accumulation is important, because this allows for identifying the
87 molecular mechanisms by which certain processes induce mutagenesis (21–23).

88 Here we present a novel, almost completely rewritten version of MutationalPatterns for the
89 analysis of mutational processes, which is easy-to-use and contains many new features,
90 such as DNA lesion segregation (24). Existing features have also been improved, resulting in
91 a very comprehensive package that can be used for both basic and more advanced
92 mutational pattern analyses. MutationalPatterns supports DBSs, multi base substitutions
93 (MBSs) and indels, and can automatically extract all these mutation types from a single
94 variant call format (VCF) file. The package can generate region specific spectra and signature
95 contributions to study the varying activities of mutational processes across the genome. The
96 package also generates more accurate results by supporting stricter signature refitting. This
97 refitting can also be bootstrapped to determine the confidence of the results. Additionally, a
98 process known as lesion segregation can be investigated.

99 The MutationalPatterns package can be used to generate novel biological insights,
100 which we demonstrate by applying it to whole genome sequencing (WGS) data obtained
101 from a lymphoblastoid cell line, in which specific DNA repair processes were deleted using
102 CRISPR-Cas9 genome editing, as well as by applying the package on large cancer datasets.

103 Additionally, we demonstrate that the package scales well on these large datasets. Finally,
104 we show the improved accuracy of the stricter signature refitting using simulated data.

105

106 **Implementation**

107 *Mutation profiles*

108 MutationalPatterns supports SBSs, DBSs, MBSs and indels. Multiple mutation types are
109 allowed to be present in a single VCF file so that users do not have to split them beforehand.
110 A specific mutation type can be selected as an argument with the “read_vcfs_as_granges”
111 function when reading in the VCF files. Alternatively, the “get_mut_type” function can be
112 used on data that is already loaded in the memory.

113 DBS and MBS variants can be called by various variant callers, such as the Genome
114 Analysis ToolKit (GATK) Mutect2, in two different ways (25). The variants can be called
115 explicitly as DBS and MBS variants or as neighboring SBSs. A downside of the first approach
116 is that neighboring germline and somatic mutations can be called as a single combined DBS
117 or MBS, because the variants are compared to the reference instead of the control sample.
118 MutationalPatterns supports both approaches. When the second approach is used,
119 neighboring SBSs will be merged into somatic DBS or MBS variants.

120 Because they get merged, DBS and MBS variants are no longer incorrectly identified
121 as separate SBSs by MutationalPatterns. This improves the quality of the SBS profiles, as
122 DBS and MBS mutations often have a very different context on account of them being
123 caused by different processes (13) (Additional file 1: Figure S1).

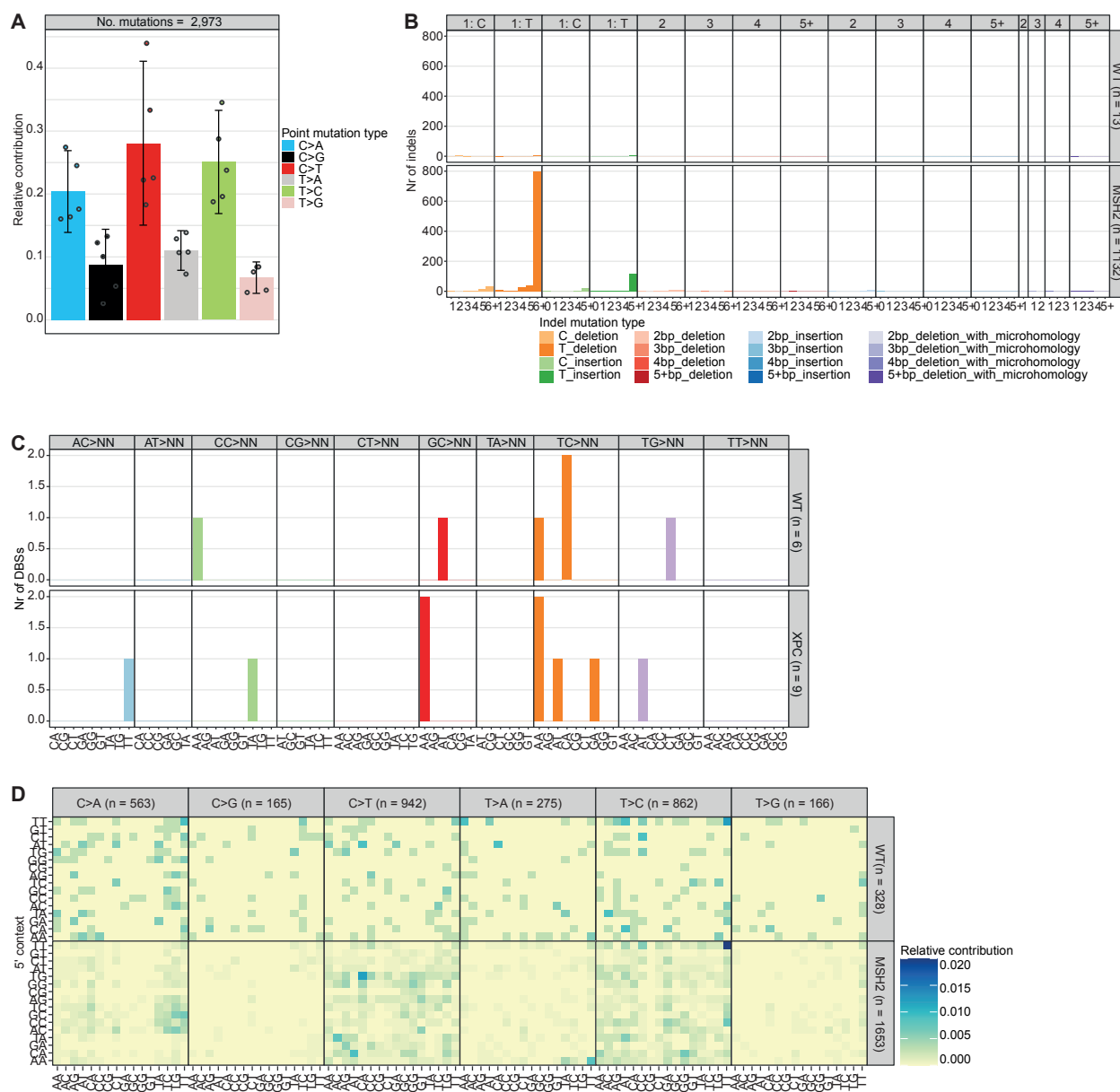
124

125 The COSMIC contexts of SBS, indel and DBS variants can be retrieved with fast vectorized
126 functions, namely “mut_context”, “get_indel_context” and “get_dbs_context”. The context
127 of SBS variants consisted of its direct 5’ and 3’ bases in the original package. These contexts
128 were chosen because they are generally the most informative and adding more bases
129 drastically increases the feature space, leading to sparsity (4). Indeed, adding only one extra
130 base to both the upstream and downstream context increases the number of features from
131 96 to 1536. However, with the increasing availability of large sequencing cohorts such large
132 feature spaces have become more manageable, making it easier to examine nucleotide
133 preference more upstream or downstream of the mutated base. Therefore,
134 MutationalPatterns’ users can now choose any context size for SBSs.

135
136 The mutation contexts can be used for custom analyses. Alternatively, the number of
137 mutations per context can be counted, resulting in a count matrix, where each row is a
138 context and each column a sample. These matrices are created with the “mut_matrix”,
139 “mut_matrix_stranded”, “count_indel_contexts”, “count_dbs_contexts” and
140 “count_mbs_contexts” functions. The “count_mbs_contexts” function uses the length of
141 the MBSs, because to date no COSMIC consensus has been defined.

142 The count matrices can be plotted as spectra or profiles for all the mutation types
143 (Fig. 1a, b, c). The SBS spectra can be displayed in the individual samples. Additionally, the
144 error bars can be displayed as standard deviation, 95% confidence interval (CI) and the
145 standard error of the mean. A count matrix with a larger context can be visualized using the
146 new “plot_profile_heatmap” or “plot_river” functions (Fig. 1d, Additional file 1: Figure S2).
147 This last function can be especially helpful to provide a quick overview of a mutation

148 spectrum with a wider context. Next to visualizing them, a count matrix can also be used for
149 downstream analyses, such as a *de novo* extraction of mutational signatures. In some cases,
150 it can be useful to pool multiple samples within a count matrix to increase statistical power.
151 This can be done using the new “pool_mut_mat” function.



152

153 Fig. 1 Mutation profiles can be made for multiple mutation types

154 a Relative contribution of the indicated mutation types to the point mutation spectrum.

155 Bars depict the mean relative contribution of each mutation type over all the samples and

156 error bars indicate the 95% confidence interval. The dots show the relative contributions of
157 the individual samples. The total number of somatic point mutations per tissue is indicated.
158 **b** Absolute contribution of the indicated mutation types to the indel spectrum for the wild-
159 type (WT) and *MSH2* knockout. The total number of indels per sample is indicated. **c**
160 Absolute contribution of the indicated mutation types to the DBS spectrum for the wild-type
161 (WT) and *XPC* knockout. The total number of DBSs per sample is indicated. **d** Heatmap
162 depicting the relative contribution of the indicated mutation types and the surrounding
163 bases to the point mutation spectrum for the WT and *MSH2* knockout. The total number of
164 somatic point mutations per tissue is indicated.

165

166 *Region specific analyses*

167 Mutational processes can be influenced by regional genomic features at multiple scales,
168 such as chromatin landscape, secondary hairpin structures as well as the major and minor
169 groove of the DNA (21–23). With the previous version of MutationalPatterns, it was possible
170 to test for enrichment and/or depletion of the mutation load in such regions. However, the
171 package lacked the possibility to automatically correct for multiple testing. In addition,
172 mutational profiles in genomic regions could not be easily assessed. In MutationalPatterns,
173 multiple testing correction is now automatically performed when testing for enrichment and
174 depletion. In addition, multiple significance levels are now supported, which can be
175 visualized using one or multiple asterisks. Furthermore, regional mutation profiles can be
176 determined in detail. This is done by first splitting mutations based on pre-defined genomic
177 regions, with the new “split_muts_region” function, which requires a GRanges or
178 GRangesList object containing chromosome coordinates as its input. These coordinates can

179 be read into R from file types like “.txt” or “.bed” files or they can be directly read from
180 databases, such as Ensembl (26). This analysis can be performed for multiple samples and
181 multiple types of regions at once. A user could, for example, split a set of mutations into
182 “promoter”, “enhancer” and “other” mutations.

183 Splitting the mutations according to different genomic regions results in a
184 GRangesList containing sample/region combinations. These combinations can be treated as
185 separate samples by, for example, performing *de novo* signature analysis to identify
186 processes that are specifically active in certain genomic regions. Knowing in which regions a
187 signature is predominantly present, can lead to a better understanding of its etiology.

188 Instead of treating the sample/region combinations as separate samples, the genomic
189 regions can also be incorporated into the mutational contexts, using the new
190 “lengthen_mut_matrix” function. This means that a mutational context like “A[C>A]A” could
191 be split into “A[C>A]A-promoter” and “A[C>A]A-enhancer”. This analysis allows users to
192 generate signatures that contain different mutation contexts in different genomic regions.

193 Such signatures could be more specific than the regular COSMIC signatures.

194 Region-specific mutation spectra can be visualized with the “plot_spectrum_region”
195 function, which contains the same arguments as the “plot_spectrum” function (Fig. 2a, b). In
196 addition, region-specific 96-channel mutation profiles can be visualized with the new
197 “plot_profile_region” function, which contains the same arguments as the “plot_96_profile”
198 function (Fig. 2c). Both the “plot_spectrum_region” and “plot_profile_region” functions
199 contain a “mode” argument, which allows users to normalize for the occurrence of the
200 different mutation types per sample/region combination, per sample, or not at all.

201 Instead of using pre-determined genomic regions, it is also possible to compare the
202 mutation spectra of regions with different mutation densities. These regions can be
203 identified using the new “bin_mutation_density” function.

204 Regional mutational patterns can also be investigated using an unsupervised
205 approach, which is unique to `MutationalPatterns`, with the new
206 “determineRegionalSimilarity” function. This function uses a sliding window approach to
207 calculate the cosine similarity between the global mutation profile and the mutation profile
208 of smaller genomic windows, allowing for the unbiased identification of regions with a
209 mutation profile, that differs from the rest of the genome. Users can correct for the
210 oligonucleotide frequency of the genomic windows using the “oligo_correction” argument.
211 The function returns an S4 object, containing the genomic windows with their associated
212 cosine similarities and the settings used to run the function. Because of the unbiased
213 approach of this function, it works best on a large dataset containing at least 100,000
214 substitutions. The result of this analysis can be visualized using the new
215 “plotRegionalSimilarity” function.

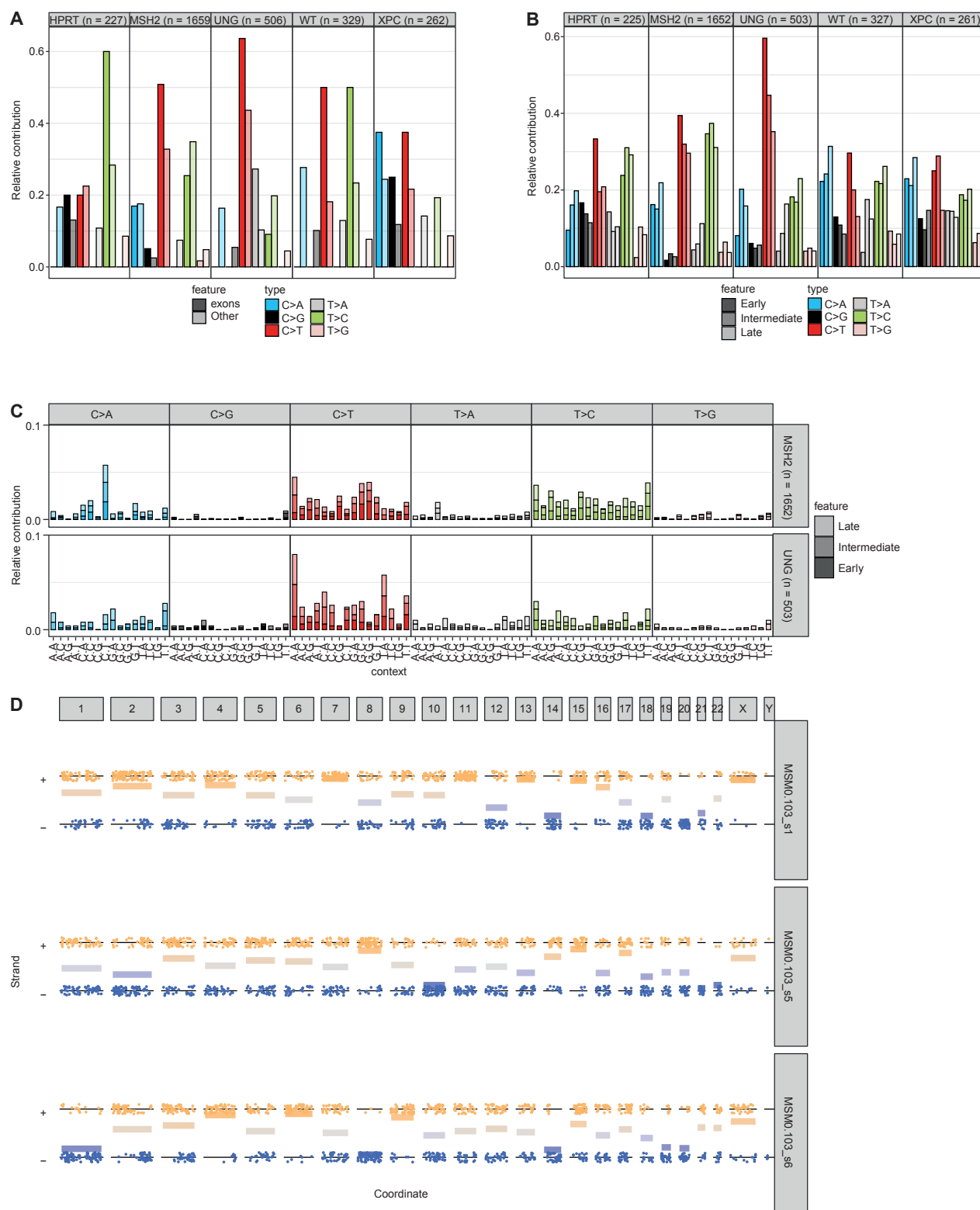
216

217 *Lesion segregation*

218 Mutation spectra sometimes contain Watson versus Crick strand asymmetries (24). These
219 asymmetries can be the result of many DNA lesions occurring during a single cell cycle. If
220 these lesions are not properly repaired before the next genome duplication, then the
221 resulting sister chromatids will segregate into different daughter cells, which will each
222 inherit the lesions on opposite strands. This process is known as lesion segregation (24). The
223 presence of lesion segregation in mutation data can be calculated with the new

224 “calculate_lesion_segregation” function. This calculation can be done for all mutations
225 together or separately for the different mutation contexts. The results can be visualized
226 using the “plot_lesion_segregation” function (Fig. 2d, Additional file 1: Figure S3).

227



228

229 Fig. 2 Regional spectra show differences between genomic regions

230 **a** Relative contribution of the indicated mutation types to the point mutation spectrum split
231 between exons and the rest of the genome for each sample. **b** Relative contribution of the

232 indicated mutation types to the point mutation spectrum split between early-,
233 intermediate-, and late-replicating DNA for each sample. **c** Relative contribution of each
234 trinucleotide change to the point mutation spectrum split between early- intermediate and
235 late-replicating DNA for each sample. **d** A jitter plot depicting the presence of lesion
236 segregation for each sample per chromosome. Each dot depicts a single base substitution.
237 Any C>N or T>N is shown as a "+" strand mutation, while G>N and A>N mutations are shown
238 on the "-" strand. The x-axis shows the position of the mutations. The horizontal lines are
239 calculated as the mean of the "+" and "-" strand, where "+" equals 1 and "-" equals 0. They
240 indicate per chromosome on which strand most of the mutations are located. The
241 mutations were downsampled to 33% to reduce the file size.

242

243 *Mutational signature analysis*

244 When performing signature analyses, it is possible to either extract novel signatures using
245 NMF or to fit previously defined signatures to a mutation count matrix (signature refitting).
246 Both approaches can be applied for all mutation types. By combining count matrices of
247 different types, it is even possible to create a composite signature.

248 MutationalPatterns now supports a variational Bayesian (Bayes) NMF algorithm from
249 the ccfindR package to help choose the optimal number of signatures, in addition to the
250 regular NMF algorithm (27) (Additional file 1: Figure S4). One challenge with *de novo*
251 signature extraction is that extracted signatures can be very similar to previously defined
252 signatures with known etiology. With the new "rename_nmf_signatures" function, these
253 extracted signatures can be identified using cosine similarity scores and their names can be

254 changed from an arbitrary naming to a custom naming that reflects their similarity to these
255 previously defined signatures.

256 The original MutationalPatterns package already contained the “fit_to_signatures”
257 function, which finds the optimal combination of signatures to reconstruct a profile and
258 calculates a reconstructed profile based on this combination of signatures. However, this
259 approach could lead to too many signatures being used to explain the data (20). One simple
260 method to reduce this overfitting, which was used in the vignette of the previous version of
261 MutationalPatterns, is to remove all signatures with less than 10 mutations. However, this
262 method, which we will call “regular_10+”, only reduced overfitting slightly. To reduce
263 overfitting, we introduce the new “fit_to_signatures_strict” function. The default backwards
264 selection method of this function iteratively refits a set of signatures to the data, each time
265 removing the signature with the lowest contribution. During each iteration the cosine
266 similarity between the original and reconstructed profile is calculated. The iteration process
267 stops when the change in cosine similarity between two iterations is bigger than the user-
268 specified “max_delta” cutoff (Additional file 1: Figure S5). Users can set the “max_delta”
269 cutoff based on their desired sensitivity and specificity. Stricter refitting, with this method, is
270 comparable to a previously described approach and results in less signatures being chosen
271 when tested on mutation data obtained from cell lines that lack specific DNA repair
272 pathways (Fig. 3a, b; see Additional file 2) (13). The “fit_to_signatures_strict” function also
273 has a best subset selection approach. This method works similarly to the backwards
274 selection approach. However, instead of removing the signature with the lowest
275 contribution, each combination of x signatures is tried. This includes signatures that were
276 not included in a previous iteration. Here, x is the number of signatures used during
277 refitting, which is reduced by one in each iteration step. By default,

278 “fit_to_signatures_strict” uses the backwards selection method, because the best subset
279 method becomes very slow when fitting against more than 10-15 signatures. Therefore, we
280 used the backwards selection method for all “strict” signature refitting analyses in the rest
281 of this manuscript. Another way to reduce overfitting is to only use signatures that are
282 known to be potentially active in your tissue/cells of interest. We recommend using this
283 method in combination with “fit_to_signatures_strict” for optimal results.

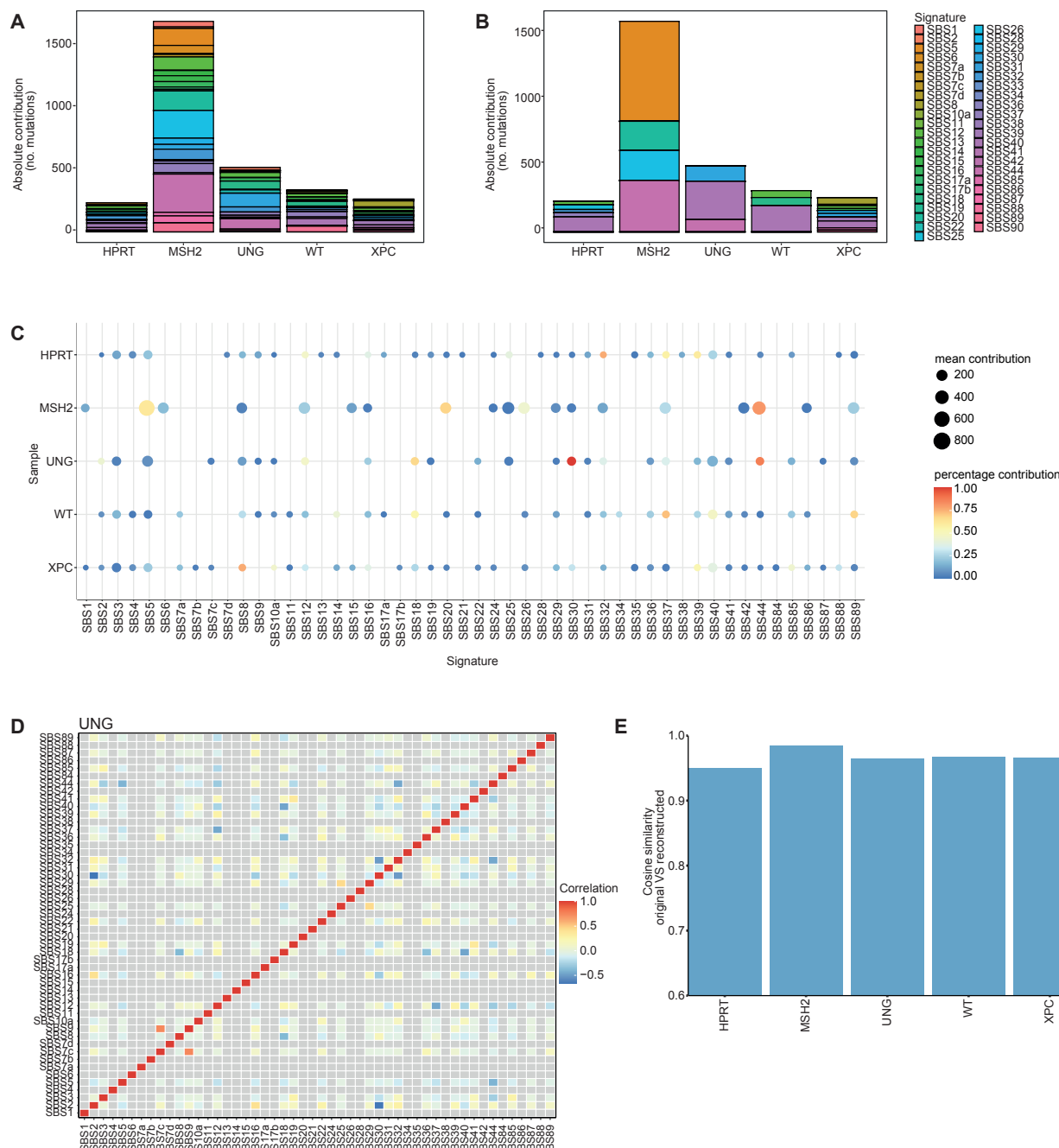
284 In addition to estimating contributions of signatures to mutation spectra, it is also
285 vital to know how confident these contributions are. The confidence of signature
286 contributions can be determined using a bootstrapping approach with the new
287 “fit_to_signatures_bootstrapped” function, which can use both the strict and the regular
288 refitting methods. Its output can be visualized in multiple ways using the
289 “plot_bootstrapped_contribution” function (Fig. 3c, Additional file 1: Figure S6). The
290 signature contributions can be correlated between signatures across the different bootstrap
291 iterations. This correlation can be visualized using the “plot_correlation_bootstrap” function
292 (Fig. 3d). A negative correlation between two signatures means that each signature had a
293 high contribution in iterations in which the other had a low contribution, which can occur
294 when the refitting process has difficulty distinguishing between two similar signatures. One
295 simple way to deal with highly similar signatures is to merge them. This can be done using
296 the new “merge_signatures” function.

297 To test the accuracy of signature analysis, the cosine similarity between the
298 reconstructed and original mutation profile needs to be determined. A high cosine similarity
299 between the reconstructed and original profile indicates that the used signatures can
300 explain the original spectrum well. This comparison between reconstructed and original

301 mutation profiles can be visualized with the new “plot_original_vs_reconstructed” function
302 (Fig. 3e).

303 In order to perform refitting, a matrix is required of the predefined signatures.
304 Signature matrices of the Catalogue of Somatic Mutations in Cancer (COSMIC) (v3.1 + v3.2),
305 SIGNAL (v1) and SparseSignatures (v1) are now included in MutationalPatterns (6,13,15,28).
306 These matrices include general, tissue-specific and drug exposure signatures. The COSMIC
307 matrices also include DBS and indel signatures, next to the standard SBS signatures.
308 Signature matrices can be easily loaded using the new “get_known_signatures” function.

309



310

311 Fig. 3 Signature refitting is improved

312 **a** Absolute contribution of each mutational signature for each sample using “regular”
 313 signature refitting and **b** “strict” signature refitting. **c** Dot plot showing the contribution of
 314 each mutational signature for each sample using bootstrapped signature refitting. The
 315 colour of a dot indicates the fraction of bootstrap iterations in which a signature
 316 contributed to a sample. The size indicates the mean number of contributing mutations

317 across bootstrap iterations in which the contribution was not zero. **d** Heatmap depicting the
318 Pearson correlation between signature contributions across the bootstrap iterations. **e** Bar
319 graph depicting the cosine similarity between the original and reconstructed profiles of each
320 sample based on signature refitting.

321

322 *Signature-specific damaging potential analysis*

323 Some signatures are more likely than others to have functional effects by causing premature
324 stop codons ("stop gain"), splice site mutations or missense mutations, because of sequence
325 specificity underlying these changes. With MutationalPatterns it is now possible to analyze
326 how likely it is for a signature to either cause "stop gain", "missense", "synonymous" or
327 "splice site" mutations for a set of genes of interest. For this analysis to be performed, the
328 potential damage first needs to be calculated per mutational context, with the
329 "context_potential_damage_analysis" function. Next, the potential damage per context is
330 combined using a weighted sum to calculate the potential damage per signature using the
331 "signature_potential_damage_analysis" function. The potential damage per signature is also
332 normalized using a "hypothetical" flat signature, which contains the same weight for each
333 mutation context.

334 This analysis will only take mutational contexts into account. Other features, such as
335 open/closed chromatin, are not considered, because they vary per tissue type. However,
336 this analysis can still give an indication of how damaging a signature might be, which could
337 be supplemented by further custom analyses.

338

339 This new version of MutationalPatterns also comes with many smaller updates and bugfixes.

340 A comprehensive list can be found in Additional file 3: Table S1.

341

342 **Results**

343

344 *Extended mutation context analysis and regional mutational patterns*

345 To demonstrate the importance of analyzing extended mutation contexts, regional

346 mutational patterns and lesion segregation for characterizing the underlying mutagenic

347 processes, we applied MutationalPatterns to three published mutation datasets. First, we

348 ran MutationalPatterns on 276 melanoma samples from the HMF database. After pooling

349 these samples, we observed that TT[C>T]CT mutations are the most common type of

350 substitution (Fig. 4a). This substitution type is more common than other T[C>T]C

351 substitutions, showing that the extended context has a large effect. Next, we compared the

352 mutation patterns of the melanoma samples between the different genomic regions

353 classified by the Ensembl regulatory build (30). While the patterns look similar, they are

354 significantly different (Fig. 4b) ($p = 0.0005$, chi-squared test). One subtle difference is the

355 low contribution of T[C>T]A in promoters compared to “Other” regions of the genome, not

356 present in the regulatory build.

357 Next, to show how MutationalPatterns can be used to identify regional activity of

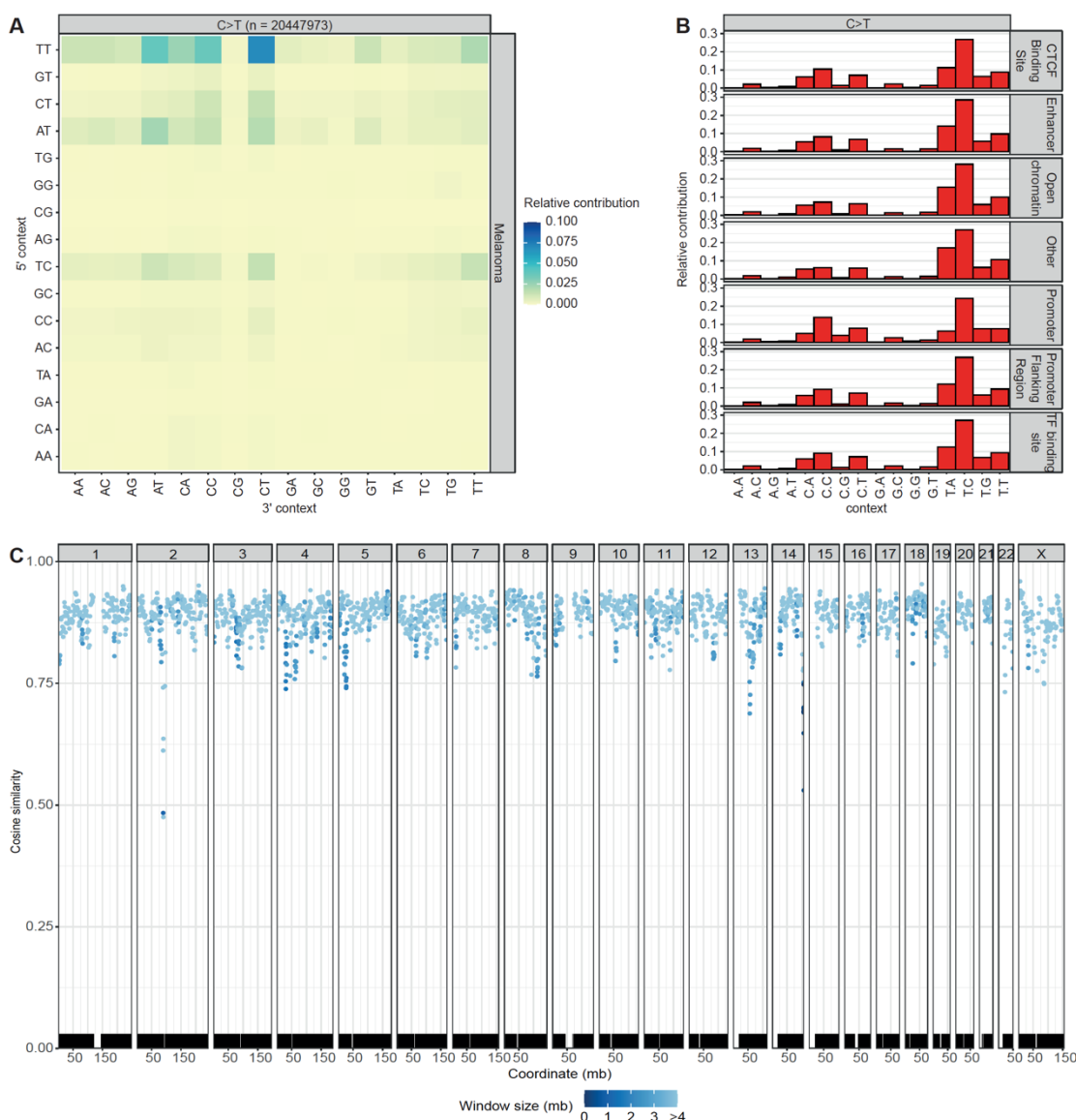
358 specific mutation processes in an unsupervised manner, we applied the package on 217

359 pooled pediatric B-ALL WGS samples (31). These B-cell-derived leukemias have undergone

360 VDJ recombination, which is associated with somatic hypermutation at loci encoding for

361 immunoglobulin (32,33). As somatic hypermutation is associated with a specific signature,
362 these sites were expected to have a mutation spectrum that is different from the rest of the
363 genome. Indeed, MutationalPatterns was able to detect this for the two VDJ regions,
364 located on chromosomes 2 and 14 (Fig. 4c). Some other regions also seem to have a
365 different mutational pattern, several of which contain PCDH genes. However, further
366 research is needed to explain these results. This example shows how MutationalPatterns
367 can identify region-specific mutational processes in an unsupervised manner.

368 Finally, to show how MutationalPatterns can identify lesion segregation, we applied
369 it on a dataset known to contain this phenomenon. We found significant lesion segregation
370 in data obtained from induced pluripotent stem cells treated with 0.109 uM of
371 dibenz[a,h]anthracene diol-epoxide (6,24), using the “plot_lesion_segregation” function of
372 MutationalPatterns (Fig. 2d). It was even possible to spot sister-chromatid-exchange events,
373 such as on chromosome 2 of sample MSM0.103_s6 (Fig. 2d, lower panel). To reduce the file
374 size of the figure, 66% of the mutations of each sample were removed using the
375 “downsample” argument of this function. Using MutationalPatterns, we also found lesion
376 segregation in patients that received the antiviral drug ganciclovir (7).



377

378 Fig. 4 Large cancer datasets show extended and regional mutation patterns

379 **a** Heatmap depicting the relative contribution of the indicated mutation types and the
380 surrounding bases to the point mutation spectrum for metastatic melanomas. The total
381 number of somatic point mutations is indicated. **b** Relative contribution of each C>T
382 trinucleotide change to the point mutation spectrum split between different genomic
383 regions. **c** Graph depicting the similarity in the mutation profile between genomic windows
384 and the rest of the genome. Each dot shows the cosine similarity between the mutation
385 profiles of a single window and the rest of the genome. The dots are colored based on the

386 sizes in mega bases of the windows. The locations of the mutations are plotted on the
387 bottom of the figure.

388

389 *MutationalPatterns offers more functionality than other mutation analysis tools*
390 An overview of the functions of MutationalPatterns and related tools is shown in Table 1.
391 The original version of MutationalPatterns is also included in this table. An important
392 advantage of the original package was that it combined many mutational analyses into a
393 single package. This new version improves many of these features and adds many new and
394 unique features.

395

396 *Mutation matrices can be generated faster*
397 To make MutationalPatterns scalable to large cancer datasets and suitable for interactive
398 analysis we improved the runtime of the “mut_matrix” and “mut_matrix_stranded”
399 functions by vectorizing them. The new functions for retrieving the mutation contexts and
400 generating the mutation matrices have also been written in a vectorized way. As a result,
401 these functions have $O(n)$ or better scaling as tested on a large WGS database from the
402 Hartwig Medical Foundation (HMF) (Additional file 1: Figure S7) (29).

403 To test their improved performance, we benchmarked the “mut_matrix” and
404 “mut_matrix_stranded” functions on the example data provided in the previous version of
405 MutationalPatterns (Additional file 1: Figure S8). These functions are now respectively 3.4
406 and 2.6 times as fast on average. In other words, a mutation matrix for 1 million SBSs can

407 now be made in only 135 seconds on a laptop, which makes these functions suitable for

408 large cancer datasets.

409

Table 1: Feature comparison with other packages

Group	Feature	Mutational Patterns	Mutational Patterns original (12)	Sigprofiler (13)	SignatureAnalyzer (13)	deconstructSigs (14)	sparseSignatures (15)	signeR (16)	somaticSignatures (17)	Maftools (18)	decompTumor2Sig (19)
Language	Language/platform	R (bioconductor)	R (bioconductor)	Python (+ R wrapper)	Python	R (cran)	R (bioconductor)	R (bioconductor)	R (bioconductor)	R (bioconductor)	R (bioconductor)
Genome	Supported genomes	Genome agnostic	Genome agnostic	Human, Mice, Rat, Yeast	-	Human	Genome agnostic	Genome agnostic	Genome agnostic	Genome agnostic	Genome agnostic
Mutation profile	96 SNV profile	X	X	X	-	X	-	X	X	X	X
	extended SNV profile	X	-	X	-	-	-	-	X	-	X
	Indel profile	X	-	X	-	-	-	-	-	-	-
	DBS profile	X	-	X	-	-	-	-	-	-	-
	MBS profile	X	-	-	-	-	-	-	-	-	-
	Transcriptional strand bias profile	X	X	X	-	-	-	-	-	-	-
	Replicative strand bias profile	X	X	X	-	-	-	-	-	-	-
	Pool samples	X	-	-	-	-	-	-	-	-	-
Signature extraction	Signature extraction (NMF)	X	X	X	-	-	-	-	X	X	-
	Signature extraction (Bayes NMF)	X	-	-	X	-	-	X	-	-	-
	Signature extraction (Lasso NMF)	-	-	-	-	-	X	-	-	-	-
	Update signature names	X	-	-	-	-	-	-	-	-	-
Signature refitting	Signature refitting	X	X	X	X	X	-	-	-	-	X
	Strict signature refitting	X	-	X	X	X	-	-	-	-	X
	Strict signature refitting (best subset)	X	-	-	-	-	-	-	-	-	X
	Bootstrapped signature refitting	X	-	-	-	-	-	-	-	-	-
	Correlation bootstrapped refitting	X	-	-	-	-	-	-	-	-	-
Signature damage analysis	Signature potential damage analysis	X	-	-	-	-	-	-	-	-	-
Signature other	Plot supported profiles / signatures	X	X	X	X	X	X	X	X	X	X
	Plot and compare supported profiles	X	X	-	-	-	-	-	-	-	-
	Signature contribution heatmap	X	X	-	-	-	-	X	X	-	-
	Signature contribution barplot	X	X	-	-	-	-	X	X	-	-
	Signature/profile similarity heatmap	X	X	-	-	-	-	-	-	X	-
	Similarity with reconstructed profile barplot	X	-	-	-	-	-	-	-	-	-
	Rainfall plot	X	X	-	-	-	-	-	X	X	-
Genomic distribution	Enrichment/depletion in genomic region	X	X	-	-	-	-	-	-	-	-
	Region specific profiles	X	-	-	-	-	-	-	-	-	-
	Region specific signatures	X	-	-	-	-	-	-	-	-	-
	Unsupervised regional similarity	X	-	-	-	-	-	-	-	-	-
Lesion segregation	Lesion segregation	X	-	-	-	-	-	-	-	-	-

410

411

412 *Strict signature refitting improves performance*

413 To determine how well the strict refitting method of MutationalPatterns performs as

414 compared to the regular method, we used simulated mutation matrices. These matrices

415 were generated by sampling trinucleotide changes of 4 different randomly selected

416 signatures. This process was repeated 300 times per matrix, to generate 300 “samples”.

417 Each of the samples in a matrix contained the same number of mutations per signature but

418 was composed of different signatures. The signatures were selected from the first 30

419 signatures of the COSMIC signature matrix. We limited our analysis to the first 30, because

420 these are the signatures that are most often observed in cancers and therefore more

421 accurately resemble real-life scenarios. In addition, this approach better resembles how the

422 package is used, because users will often fit against a limited number of signatures

423 associated with a specific tissue. By limiting ourselves to the first 30 COSMIC signatures we

424 also reduced overfitting. Any overfitting we observed was thus not caused by us using an

425 unusually large signature matrix. In total we generated 4 matrices, each containing 300

426 samples. The number of mutations per sample was respectively 200, 400, 2000 and 4000 for

427 the 4 different matrices.

428 The fraction of correctly attributed mutations to the specific signatures was

429 increased with the strict refitting approach of MutationalPatterns as compared to “regular”

430 or “regular_10+” refitting (Additional file 1: Figure S9a). All the tested refitting methods

431 work better when there are more mutations per signature. Instead of using the number of

432 correctly attributed mutations as a readout for performance, we determined whether the

433 presence and absence of specific signatures was correctly classified. This readout might be

434 more informative for mutational signature analysis because the presence of a signature can
435 be a clinically relevant finding. The strict refitting method achieved a much higher precision
436 than the original methods, while retaining a high correct recall rate (sensitivity) (Additional
437 file 1: Figure S9b). The strict method obtained an area under the curve (AUC) of 0.925, even
438 when only 50 mutations were present per signature, indicating that refitting can be
439 performed on relatively small amounts of mutations.

440

441 *SBS10a and SBS18 have a high damage potential*

442 We applied the “signature_potential_damage_analysis” function on the COSMIC signatures.
443 This analysis showed that SBS10a and SBS18 are respectively 3.6 and 2.0 times as likely to
444 cause a “stop gain” mutation compared to a completely flat signature, containing the same
445 weight for each mutation context, on a set of genes associated with cancer (Additional file
446 3: Table S2, Table S3). SBS18 is related to oxidative stress, suggesting that this type of stress
447 has a high potency of generating premature stop codons in genes that are recurrently
448 associated with tumorigenesis (13). In contrast, the clock-like signature SBS1, which also
449 occurs in healthy cells, was 0.81 and 0.40 times as likely to cause “stop gain” and “splice
450 site” mutations, respectively, as compared to a completely flat hypothetical signature (2,34)
451 (Additional file 3: Table S2). The damaging potential of this ageing-related mutational
452 process is thus relatively low. Overall, C>A heavy signatures, like the recently identified
453 ganciclovir signature, have more damage potential, because they are most likely to
454 introduce a premature stop codon in an open reading frame (7). Being able to quickly assess
455 the damage potential of existing and novel signatures can be very useful to prioritize
456 samples and mutagenic exposures for further investigation.

457

458 *Applying MutationalPatterns on mutation data of DNA repair-deficiencies*

459 To illustrate the functionality of MutationalPatterns on real-life data and to obtain novel

460 biological insights, we applied it to mutation data obtained from cell lines in which we

461 deleted specific DNA repair pathways using CRISPR-Cas9 genome editing technology

462 (Additional file 1: Figure S10, Additional file 2). In AHH-1 cells, a lymphoblastoid cell line, we

463 generated bi-allelic knockout lines of *MSH2*, *UNG* and *XPC* by transfecting the cells with a

464 plasmid containing Cas9 and a single gRNA against the gene of interest. By co-transfection

465 with a *HPRT*-targeting plasmid, we were able to select the transfected cells using 6-

466 thioguanine, to which only HPRT-sufficient cells are sensitive. Using this protocol, no

467 targeting vectors for each gene of interest were required. We analyzed somatic mutations in

468 *HPRT*-only knockout lines as well as the combination of *HPRT* with *MSH2*, *UNG* and *XPC*

469 (Additional file 2). To catalogue mutations that were acquired specifically in the absence of

470 the targeted DNA repair gene, we used a previously developed method (35). In brief, whole

471 genome sequencing was performed on generated clones and subclones. By subtracting

472 variants present in the clones from those in the subclones, the somatic mutations, that

473 accumulated in between the clonal steps, were determined.

474

475 The SBS profiles are shown in Additional file 1: Figure S11. Interestingly, the profile observed

476 in the *MSH2* knockout cell line displayed a large C[C>A]T peak. When extending the

477 sequence context surrounding the mutated base, the *MSH2* deficiency profile showed a

478 large TT[T>C]TT peak, suggesting that this extended context surrounding mutated thymine

479 residues is important for the underlying mutagenic process (Fig. 1d).

480

481 Next, we examined regional mutation patterns. The spectra of the *MSH2*- and *UNG*-
482 deficient cells varied between the exonic regions and the rest of the genome (Fig. 2a)(fdr =
483 0.0012, fdr = 0.0012; chi-squared test). Their exons contained more C>T and less T>C
484 mutations. The other samples did not show a significant difference in regional mutation
485 spectra. However, when we downsampled all the samples to 227 mutations, which is the
486 number of mutations in the *HPRT* only knockout, no significant regional mutation patterns
487 were observed in *MSH2* and *UNG* knockout cells. This suggests that with this number of
488 mutations insufficient statistical power was obtained for these analyses. Next to examining
489 mutation profiles in exonic regions, we also analyzed regions with different replication
490 timing dynamics, using the median replication timing data from 5 B-lymphocyte cell lines
491 from ENCODE (Fig. 2b, Additional file 3: Table S4) (40). The spectra of *MSH2* and *UNG*
492 knockouts were different between early-, intermediate- and late-replicating DNA (fdr =
493 0.0012, fdr = 0.0012; chi-squared test). Early replicating DNA has more C>T and less C>A
494 than late replicating DNA. These differences were still present when downsampling was
495 applied (fdr = 0.0025, fdr = 0.010; chi-squared test). Based on these region-specific analyses,
496 we can conclude that the mutational processes active in the *MSH2* and *UNG* knockouts
497 show varying activities in different regions of the genome, a result that cannot easily be
498 obtained with other tools.

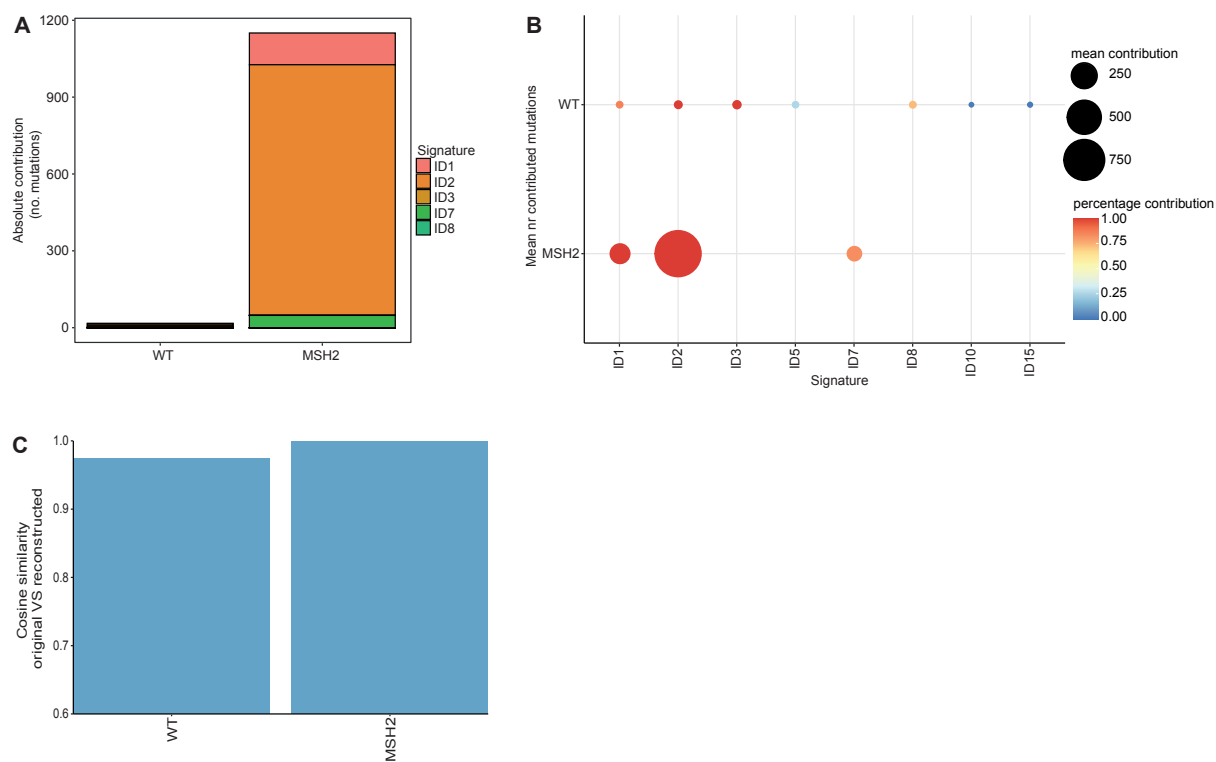
499 We also tested if any of the DNA repair knockout cells displayed lesion segregation,
500 which would indicate that most of the mutations occurred during a single cell-cycle;
501 however, this was not the case (Additional file 1: Figure S6).

502

503 Finally, we looked at the mutational signatures in the knockout samples. Based on signature
504 refitting, the *MSH2* knockout contained contributions of SBS5, SBS20, SBS26 and SBS44 (Fig.
505 3b, c). Because of the bootstrapping we can be more confident in these results. SBS5 is a
506 clock-like signature, with unknown etiology. SBS20, SBS26 and SBS44 are all associated with
507 defective DNA mismatch repair in cancer mutation data (13). The *UNG* knockout contained
508 contributions from SBS30, which has previously been attributed to deficiency of the base
509 excision repair gene *NTHL1* (13). The glycosylase encoded by *NTHL1* is involved in the
510 removal of oxidized pyrimidines from the DNA and therefore SBS30 likely reflects an
511 alternative consequence of oxidative stress-induced mutagenesis as compared to SBS18.
512 However, *UNG* is a glycosylase that is believed to remove uracil residues from the DNA
513 (36,37). Therefore, our data suggests that SBS30 can be caused, besides oxidized
514 pyrimidines, by unremoved uracil residues. Alternatively, *UNG* may also, to a certain extent,
515 be involved in the removal of oxidized pyrimidines from the DNA. Even though the
516 contribution of SBS30 was relatively modest in the *UNG* knockout, it was consistently picked
517 up by the bootstrapping algorithm. This observation indicated that the number of mutations
518 attributed to a signature is not necessarily related to the confidence of its presence, which
519 further demonstrates the importance of our bootstrapping approach. Unexpectedly, the
520 contribution of SBS30 in *UNG* knockout cells was negatively correlated with SBS2, even
521 though their cosine similarity is only 0.46 (Fig. 3d). This indicates that the refitting algorithm
522 has difficulty choosing between SBS2 and SBS30. Such difficulties in signature selection
523 could lead to different and possibly incorrect signatures being attributed to similar sample
524 types. Understanding the correlation of estimated signature contributions between
525 different signatures, which can be achieved with bootstrapping, is important to prevent
526 incorrect interpretation of the data. The *XPC* knockout contained contributions from SBS8.

527 The etiology of this signature is not yet known. However, this finding further confirms the
528 association of SBS8 with nucleotide excision repair deficiency (38,39). Overall, the COSMIC
529 signatures could explain the mutation profiles of most samples quite well, even when strict
530 refitting was used (Fig. 3e).

531 Next, we studied the indel signatures in these knockout lines. Deletion of *MSH2*
532 resulted in an increased number of indels as compared to wild-type cells (Fig. 1b). Most of
533 these indels were single thymine deletions in thymine mononucleotide repeat regions.
534 Signature analysis indicated that ID1, ID2 and ID7 contributed to the indel pattern in the
535 *MSH2*-deficient cells (Fig. 5a, b). Of these, ID1 and ID2 are associated with polymerase
536 slippage during DNA replication and found in large numbers in cancers with mismatch repair
537 deficiency. ID7 is also associated with defective DNA mismatch repair, but not attributed to
538 polymerase slippage (13). Together these signatures could explain the mutational indel
539 profile of *MSH2* knockout cells very well (Fig. 5c), showing that MutationalPatterns can
540 perform indel signature refitting. None of the knockout cells displayed a strongly increased
541 number of DBSs as compared to the wild-type cells (Fig. 1c).



542

543 Fig. 5 Indel signatures can explain the *MSH2* profile

544 **a** Relative contribution of each mutational signature for the wild-type (WT) and *MSH2*
545 samples using strict signature refitting. **b** Dot plot showing the contribution of each
546 mutational signature for the WT and *MSH2* samples using bootstrapped signature refitting.
547 The color of a dot indicates the fraction of bootstrap iterations in which a signature
548 contributed to a sample. The size indicates the mean number of contributing mutations
549 across bootstrap iterations in which the contribution was not zero. **c** Bar graph depicting the
550 cosine similarity between the original and reconstructed profiles of the WT and *MSH2*
551 samples based on signature refitting.

552

553 **Discussion**

554 The novel version of MutationalPatterns has been designed to be easy-to-use in such a way
555 that both experienced bioinformaticians and wet-lab scientists with a limited computational
556 background can use it. The code is written in the tidyverse style, which makes it more
557 similar to natural English and therefore easier to understand for non-programmers.
558 MutationalPatterns gives clear error messages with tips on how to solve them, in contrast to
559 the default error messages in R, which can sometimes be cryptic. The updated vignette,
560 accompanying the package, not only explains how the functions in the package can be used,
561 but also informs users on the pros and cons of the different analysis strategies.

562 Similar to the previous version of the package, plots are all generated using ggplot2
563 (41). This allows users to visualize their data in highly customizable plots that can be easily
564 modified. Because this feature was not readily apparent for many users of the original
565 MutationalPatterns package, we have now explicitly showed how to modify the elements of
566 a plot, such as the axis and theme, in the vignette.

567 We have adopted unit testing for this version of the package, resulting in more than
568 90% code coverage. This will improve the stability of the package and makes it easier to
569 maintain.

570 The novel version of MutationalPatterns is already available on Bioconductor as an
571 update of the previous version. MutationalPatterns does not break existing scripts and
572 pipelines, because backwards incompatible changes have been kept to a minimum.

573

574 **Conclusions**

575 MutationalPatterns is an easy-to-use R/Bioconductor package that allows in-depth analysis
576 of a broad range of patterns in somatic mutation catalogues, supporting single and double
577 base substitutions as well as small insertions and deletions. Here, we have described the
578 new and improved features of the package and shown how the package performs on
579 existing cancer data sets and on mutation data obtained from cell lines in which specific
580 DNA repair genes are deleted. These analyses demonstrate how the package can be used to
581 generate novel biological insights.

582

583 Mutational pattern analyses have proven to be a powerful approach to dissect mutational
584 processes that have operated in cancer and to support treatment decision making in
585 personalized medicine. Therefore, mutational patterns hold a great promise for improved
586 future cancer diagnosis. The MutationalPatterns package can be used to fulfill this promise
587 and we are confident that it will be embraced by the community.

588

589 **Availability and requirements**

590 The availability and requirements are listed as follows:

591 Project name: MutationalPatterns

592 Project home page: <https://github.com/ToolsVanBox/MutationalPatterns>

593 Archived version:

594 <https://bioconductor.org/packages/3.14/bioc/html/MutationalPatterns.html>

595 Operating system(s): Linux, Windows or MacOS

596 Programming language: R (version > = 4.1.0)

597 License: MIT

598

599 **List of abbreviations**

600 HR: homologous recombination

601 Indels: Insertions and deletions

602 DBS: double base substitutions

603 VCF: variant call format

604 MBS: Multi base substitutions

605 COSMIC: Catalogue of Somatic Mutations in Cancer

606 NMF: non-negative matrix factorization

607 Bayes: Bayesian

608 AUC: Area under the curve

609 PCA: Principal component analysis

610 CI: Confidence interval

611 WT: wild-type

612 Mb: mega bases

613

614 **Declarations**

615 *Ethics approval and consent to participate*

616 Not applicable

617

618 *Consent for publication*

619 Not applicable

620

621 *Availability of data and materials*

622 The datasets supporting this article are available on EGA under accession number (Study ID
623 EGAS00001004789).

624 Additionally, the VCF files and scripts that can be used to reproduce all figures in this paper
625 can be found at

626 https://github.com/ToolsVanBox/MutationalPatterns_manuscript2_data_scripts/

627

628 *Competing interests*

629 The authors declare that they have no competing interests.

630

631 *Funding*

632 This work was financially supported by a NWO VIDI grant project 016.Vidi.171.023 to R.v.B.

633

634 Authors' contributions

635 F.M., R.v.B. and A.M.B wrote the manuscript. F.M. and J.d.K. developed and implemented
636 the package. F.M. and R.O. maintain the package. A.M.B. and M.V. generated the data. F.M.
637 and M.J.v.R. analyzed the data. A.v.H., B.v.d.R. and E.C. tested the package and provided
638 feedback. All authors read and approved the final manuscript.

639

640 *Acknowledgements*

641 We would like to thank Francis Blokzijl and Roel Janssen for developing and maintaining the
642 first version of this package. We also want to thank Roel Janssen for his support during the
643 handover of the package. Finally, we would like to thank anybody who tested the package
644 for their feedback.

645

646 **References**

- 647 1. Helleday T, Eshtad S, Nik-Zainal S. Mechanisms underlying mutational signatures in
648 human cancers. *Nat Rev Genet.* 2014;15:585–98.
- 649 2. Blokzijl F, de Ligt J, Jager M, Sasselli V, Roerink S, Sasaki N, et al. Tissue-specific
650 mutation accumulation in human adult stem cells during life. *Nature.* 2016;538:260–
651 4.
- 652 3. Campbell PJ, Getz G, Korbel JO, Stuart JM, Jennings JL, Stein LD, et al. Pan-cancer
653 analysis of whole genomes. *Nature [Internet].* 2020;578(7793):82–93. Available from:
654 <https://doi.org/10.1038/s41586-020-1969-6>

655 4. Alexandrov LB, Nik-Zainal S, Wedge DC, Campbell PJ, Stratton MR. Deciphering
656 Signatures of Mutational Processes Operative in Human Cancer. *Cell Rep.*
657 2013;3:246–59.

658 5. Pleguezuelos-Manzano C, Puschhof J, Rosendahl Huber A, van Hoeck A, Wood HM,
659 Nomburg J, et al. Mutational signature in colorectal cancer caused by genotoxic pks+
660 E. coli. *Nature.* 2020;580:269–73.

661 6. Kucab JE, Zou X, Morganella S, Joel M, Nanda AS, Nagy E, et al. A Compendium of
662 Mutational Signatures of Environmental Agents. *Cell.* 2019;177:821-836.e16.

663 7. de Kanter JK, Peci F, Bertrums E, Rosendahl Huber A, van Leeuwen A, van Roosmalen
664 MJ, et al. Antiviral treatment causes a unique mutational signature in cancers of
665 transplantation recipients. *Cell Stem Cell* [Internet]. 2021; Available from:
666 <https://www.sciencedirect.com/science/article/pii/S1934590921003374>

667 8. Davies H, Glodzik D, Morganella S, Yates LR, Staaf J, Zou X, et al. HRDetect is a
668 predictor of BRCA1 and BRCA2 deficiency based on mutational signatures. *Nat Med.*
669 2017;23:517–25.

670 9. Nguyen L, W. M. Martens J, Van Hoeck A, Cuppen E. Pan-cancer landscape of
671 homologous recombination deficiency. *Nat Commun.* 2020;11:5584.

672 10. Bryant HE, Schultz N, Thomas HD, Parker KM, Flower D, Lopez E, et al. Specific killing
673 of BRCA2-deficient tumours with inhibitors of poly(ADP-ribose) polymerase. *Nature.*
674 2005;434:913–7.

675 11. Fong PC, Boss DS, Yap TA, Tutt A, Wu P, Mergui-Roelvink M, et al. Inhibition of
676 Poly(ADP-Ribose) Polymerase in Tumors from BRCA Mutation Carriers. *N Engl J Med.*

677 2009;361:557–68.

678 12. Blokzijl F, Janssen R, van Boxtel R, Cuppen E. MutationalPatterns: comprehensive
679 genome-wide analysis of mutational processes. *Genome Med.* 2018;

680 13. Alexandrov LB, Kim J, Haradhvala NJ, Huang MN, Tian Ng AW, Wu Y, et al. The
681 repertoire of mutational signatures in human cancer. *Nature.* 2020;578:94–101.

682 14. Rosenthal R, McGranahan N, Herrero J, Taylor BS, Swanton C. deconstructSigs:
683 delineating mutational processes in single tumors distinguishes DNA repair
684 deficiencies and patterns of carcinoma evolution. *Genome Biol.* 2016;17:31.

685 15. Ramazzotti D, Lal A, Liu K, Tibshirani R, Sidow A. De Novo Mutational Signature
686 Discovery in Tumor Genomes using SparseSignatures. *bioRxiv.* 2019;384834.

687 16. Rosales RA, Drummond RD, Valieris R, Dias-Neto E, Da Silva IT. signeR: An empirical
688 Bayesian approach to mutational signature discovery. *Bioinformatics.* 2017;33:8–16.

689 17. Gehring JS, Fischer B, Lawrence M, Huber W. SomaticSignatures: Inferring mutational
690 signatures from single-nucleotide variants. *Bioinformatics.* 2015;31:3673–5.

691 18. Mayakonda A, Lin D-C, Assenov Y, Plass C, Koeffler HP. Maftools: efficient and
692 comprehensive analysis of somatic variants in cancer. *Genome Res.* 2018/10/19. 2018
693 Nov;28:1747–56.

694 19. Krüger S, Piro RM. decompTumor2Sig: identification of mutational signatures active
695 in individual tumors. *BMC Bioinformatics* [Internet]. 2019;20(4):152. Available from:
696 <https://doi.org/10.1186/s12859-019-2688-6>

697 20. Maura F, Degasperi A, Nadeu F, Leongamornlert D, Davies H, Moore L, et al. A

698 practical guide for mutational signature analysis in hematological malignancies. *Nat*
699 *Commun.* 2019;10:2969.

700 21. Polak P, Karlic R, Koren A, Thurman R, Sandstrom R, Lawrence MS, et al. Cell-of-origin
701 chromatin organization shapes the mutational landscape of cancer. *Nature.*
702 2015;518:360–4.

703 22. Buisson R, Langenbucher A, Bowen D, Kwan EE, Benes CH, Zou L, et al. Passenger
704 hotspot mutations in cancer driven by APOBEC3A and mesoscale genomic features.
705 *Science (80-).* 2019;364:eaaw2872.

706 23. Gonzalez-Perez A, Sabarinathan R, Lopez-Bigas N. Local Determinants of the
707 Mutational Landscape of the Human Genome. *Cell.* 2019;177:101–14.

708 24. Aitken SJ, Anderson CJ, Connor F, Pich O, Sundaram V, Feig C, et al. Pervasive lesion
709 segregation shapes cancer genome evolution. *Nature.* 2020;583:265–70.

710 25. Benjamin D, Sato T, Cibulskis K, Getz G, Stewart C, Lichtenstein L. Calling Somatic
711 SNVs and Indels with Mutect2. *bioRxiv.* 2019;861054.

712 26. Yates AD, Achuthan P, Akanni W, Allen J, Allen J, Alvarez-Jarreta J, et al. Ensembl
713 2020. *Nucleic Acids Res.* 2020;48:D682–8.

714 27. Woo J, Winterhoff BJ, Starr TK, Aliferis C, Wang J. De novo prediction of cell-type
715 complexity in single-cell RNA-seq and tumor microenvironments. *Life Sci Alliance.*
716 2019;2:e201900443.

717 28. Degasperi A, Amarante TD, Czarnecki J, Shooter S, Zou X, Glodzik D, et al. A practical
718 framework and online tool for mutational signature analyses show inter-tissue
719 variation and driver dependencies. *Nat cancer.* 2020;1:249–63.

720 29. Priestley P, Baber J, Lolkema MP, Steeghs N, de Bruijn E, Shale C, et al. Pan-cancer
721 whole-genome analyses of metastatic solid tumours. *Nature*. 2019;575:210–6.

722 30. Zerbino DR, Wilder SP, Johnson N, Juettemann T, Flieck PR. The ensembl regulatory
723 build. *Genome Biol* [Internet]. 2015 Mar;16:56. Available from:
724 <http://europepmc.org/articles/PMC4407537>

725 31. Ma X, Liu Y, Liu Y, Alexandrov LB, Edmonson MN, Gawad C, et al. Pan-cancer genome
726 and transcriptome analyses of 1,699 paediatric leukaemias and solid tumours.
727 *Nature*. 2018 Feb;

728 32. Chi X, Li Y, Qiu X. V(D)J recombination, somatic hypermutation and class switch
729 recombination of immunoglobulins: mechanism and regulation. *Immunology*
730 [Internet]. 2020/02/27. 2020 Jul;160(3):233–47. Available from:
731 <https://pubmed.ncbi.nlm.nih.gov/32031242>

732 33. Di Noia JM, Neuberger MS. Molecular Mechanisms of Antibody Somatic
733 Hypermutation. *Annu Rev Biochem* [Internet]. 2007 Jun 7;76(1):1–22. Available from:
734 <https://doi.org/10.1146/annurev.biochem.76.061705.090740>

735 34. Alexandrov LB, Jones PH, Wedge DC, Sale JE, Campbell PJ, Nik-Zainal S, et al. Clock-
736 like mutational processes in human somatic cells. *Nat Genet*. 2015;47:1402–7.

737 35. Drost J, van Boxtel R, Blokzijl F, Mizutani T, Sasaki N, Sasselli V, et al. Use of CRISPR-
738 modified human stem cell organoids to study the origin of mutational signatures in
739 cancer. *Science* (80-). 2017;238:eaao3130.

740 36. Prasad A, Wallace SS, Pederson DS. Initiation of Base Excision Repair of Oxidative
741 Lesions in Nucleosomes by the Human, Bifunctional DNA Glycosylase NTH1. *Mol Cell*

742 Biol. 2007;27:8442 LP – 8453.

743 37. Li J, Braganza A, Sobol RW. Base Excision Repair Facilitates a Functional Relationship

744 Between Guanine Oxidation and Histone Demethylation. Antioxid Redox Signal.

745 2013;18:2429–43.

746 38. Jager M, Blokzijl F, Kuijk E, Bertl J, Vougioukalaki M, Janssen R, et al. Deficiency of
747 nucleotide excision repair is associated with mutational signature observed in cancer.

748 Genome Res. 2019;29:1067–77.

749 39. Yurchenko AA, Padoleau I, Matkarimov BT, Soulier J, Sarasin A, Nikolaev S. XPC
750 deficiency increases risk of hematologic malignancies through mutator phenotype
751 and characteristic mutational signature. *Nat Commun* [Internet]. 2020;11(1):5834.

752 Available from: <https://doi.org/10.1038/s41467-020-19633-9>

753 40. Moore JE, Purcaro MJ, Pratt HE, Epstein CB, Shores N, Adrian J, et al. Expanded
754 encyclopaedias of DNA elements in the human and mouse genomes. *Nature*.
755 2020;583:699–710

756 41. Wickham H. *ggplot2: Elegant Graphics for Data Analysis*. Springer-Verlag New York;
757 2016

758

759 Additional file 1:

760 PDF (pdf)

761 Additional figures

762 A PDF file containing the additional figures

763

764 Additional file 2:

765 PDF (.pdf)

766 Additional methods

767 A PDF file describing the generation and sequencing analysis of the knockout lines.

768

769 Additional file 3:

770 Excel (.xlsx)

771 Additional tables

772 An Excel file containing the additional tables.